Molecular Dynamics Simulations of Electric Field Poled Nonlinear Optical Chromophores Incorporated in a Polymer Matrix

M. Makowska-Janusik,*,† H. Reis,* and M. G. Papadopoulos*

Institute of Organic and Pharmaceutical Chemistry, National Hellenic Research Foundation, Vasileos Constantinou 48, GR-11635 Athens, Greece

I. G. Economou and N. Zacharopoulos

Molecular Modeling of Materials Laboratory, Institute of Physical Chemistry, National Research Center for Physical Sciences "Demokritos", GR 15310 Aghia Paraskevi Attikis, Greece

Received: July 28, 2003; In Final Form: October 1, 2003

The electric field poling process of nonlinear optical chromophores embedded in an amorphous polymer matrix was studied using molecular dynamics (MD) simulations. Three systems were considered, consisting of a poly(methyl methacrylate) matrix doped with the following chromophores: *N*,*N*-dimethyl-*p*-nitroaniline (DPNA), 4-(dimethylamino)-4′-nitrostilbene (DMANS), and *N*,*N*′-di-*n*-propyl-2,4-dinitro-1,5-diaminobenzene (DPDNDAB). The cooling process in the presence of a poling electric field was simulated at constant NPT conditions using simulated annealing. The rotational dynamics of the dopants was investigated in the unpoled and poled states above T_g and in the poled state below T_g. The short-time behavior with respect to the back-relaxation to the unpoled state following removal of the poling field was examined for the systems below T_g and was found to deviate from the single-exponential model. The electric field effects, during and following poling, were examined by computing the angle between the dipole moment of the chromophores and the external electric field. MD simulations at temperatures in the vicinity of T_g revealed that during the simulated phase transition from the liquid state to the glassy structure the degree of alignment remained constant. The dependence of back-relaxation to the unpoled glassy state on the chromophores was investigated. DPNA molecules were found to be in closer proximity to the side groups than to the backbone units of the polymer at both temperatures, in contrast to DMANS at both temperatures and to DPDNDAB in the glassy state. The radial distribution functions for all systems are typical of amorphous structures. The reorientation of chromophores exhibits a higher degree of correlation with the facile motion of the PMMA side groups than with the configurational motion along the polymer backbone. The degree of chromophore alignment depends on its size and distance from the side groups of the polymer.

Introduction

Organic and polymeric systems are now being intensively studied because of their potential applications in optoelectronic and all-optical computing devices.[1] These systems possess many advantages over inorganic systems.[2] Organic molecules involving a conjugated π-electron system terminated with donor and acceptor groups show large hyperpolarizabilities.[3,4] Amorphous polymers involving dopant molecules with large first hyperpolarizabilities show interesting nonlinear optical (NLO) properties, for example second harmonic generation (SHG).[5,6] A prerequisite for SHG is a noncentrosymmetrical arrangement of the NLO active molecules in the polymer matrix.[7] One way to obtain a large and persistent SHG effect is to dope an amorphous polymer with organic donor−acceptor molecules and to induce a polar orientation by an electric field,[8,9] at temperatures where the matrix is sufficiently mobile to allow fast alignment of the dopant molecules, i.e., above its glass transition temperature T_g. The sample is then cooled below T_g in the presence of the poling field in order to stabilize the noncentrosymmetrical arrangement against back-relaxation to the random orientational distribution.[10]

The polar orientation order parameters associated with SHG of poled polymers doped with one-dimensional NLO chromophores are $\langle\cos\theta\rangle$ and $\langle\cos^3\theta\rangle$, where θ is the angle between the molecular dipole moment and the poling electric field, while the angular brackets denote an ensemble average in the presence of the external electric field. The parameters $\langle\cos\theta\rangle$ and $\langle\cos^3\theta\rangle$ can be studied by dipolar orientation dynamics and the relaxation behavior of the NLO chromophores inside the polymer matrix. The computed order parameters $\langle\cos\theta\rangle$ and $\langle\cos^3\theta\rangle$ may be compared with the theoretically predicted odd-order Langevin functions $L_1(p)$ and $L_3(p)$.[11] The dynamics of the polymer chain motion also strongly influences the SHG signal.[12] The nature of the relaxation behavior of the second-order NLO response with regard to the polymer chain motion and the disorder of chromophores, following removal of the electric field, has been the subject of intense research recently.[13−24] The decay of the SHG intensity reflects the temporal stability of the macroscopic second-order susceptibility $\chi^{(2)}$, which depends mainly on the orientation of the chromophores. An important issue in this context is the coupling of the dopant's reorientation to the structural or α-relaxation of the host matrix.

* Corresponding authors. E-mail: m.makowska@wsp.czest.pl (M.M.-J.); hreis@eie.gr (H.R.); mpapad@eie.gr (M.G.P.).

† Permanent address: Institute of Physics, WSP, Al Armii Krajowej 13/15, PL-42201 Częstochowa, Poland.

10.1021/jp036197+ CCC: $27.50
Published on Web 12/16/2003

An additional issue arises from the occurrence of local free volume, in which the molecules can rotate freely.

Several models have been proposed to describe the mobility of chromophores hosted in polymers; for example, one may note the single-exponential model due to Debye,[25] the stretched exponential approach by Kohlrausch−Williams−Watts (KWW),[26,27] the biexponential and triexponential approach,[28] and the Liu−Ramkrishna−Lackritz (LRL) model.[29] Experimental data show that the single-exponential model does not fully describe the time dependence observed for doped polymers.[30] Even for systems of identical dopant species, the microenvironment of individual constituents is not expected to be similar, so researchers have combined the individual relaxation times into two or three distinct representative relaxation times,[12] or even used a continuous distribution of relaxation times, as in the KWW model.[19]

In the present work fully atomistic simulations were performed on three electric field poled host−guest polymer systems, consisting of a poly(methyl methacrylate) (PMMA) matrix as host, doped with different chromophores, namely, *N*,*N*-dimethyl-*p*-nitroaniline (DPNA), 4-(dimethylamino)-4′-nitrostilbene (DMANS), and *N*,*N*′-di-*n*-propyl-2,4-dinitro-1,5-diaminobenzene (DPDNDAB). Kim and Hayden[11] have used simulations to study static conformational properties, radial distribution functions, and polymer mobility in the poled and unpoled PMMA/DPNA system. They have shown that the PMMA matrix strongly affects the mobility of chromophores and that the poling field influences both dopant and polymer mobilities. In their approach, two systems were prepared with different densities corresponding to states above and below the glass transition temperature T_g. These systems were then subjected to a poling field.

We have applied a different approach in that we use simulated annealing to model the cooling process in the presence of the poling field. This allows for a more direct comparison of the systems above and below T_g. The price to pay for this is that, due to the very high cooling rates of the simulation as compared to the experimental conditions, the systems do not relax fully to the sub-T_g steady state. To achieve a degree of alignment corresponding to a steady state within the time scale accessible to molecular dynamics, the simulations were performed under high-strength electric fields. This artifact reduces somehow the comparability of the results of the molecular dynamic (MD) simulations with the experimental measurements. We further extend the work of Kim and Hayden by investigating the orientational relaxation of the guest molecules following removal of the poling field in the glassy state. Additionally, we study three different NLO molecules as dopants in order to investigate size and shape effects. Apart from the relatively compact DPNA, which is a derivative of the "classic" donor−acceptor chromophore *p*-nitroaniline,[31] we used the larger molecule DMANS with a semirigid, rodlike shape, and DPDNDAB, with a more disklike shape and increased internal flexibility due to the attached alkyl chains. DPDNDAB is furthermore a two-dimensional NLO chromophore,[32] in contrast to the one-dimensional NLO chromophores DPNA and DMANS. The system PMMA/DMANS has been the subject of several experimental investigations concerning, e.g., the chromophore rotational dynamics, local polymer dynamics, and NLO properties.[6,13,28,29,33,34] The different size of the selected chromophores allows for the determination of the dynamic distribution of the local free volume in the investigated systems.

This work is expected to provide insight into the dynamics of the reorientation of DPNA, DMANS, and DPDNDAB in the amorphous matrix and in changes induced by the microenvironment surrounding the dopant. The study of chromophore reorientation in a doped polymer matrix is of considerable interest, because it provides information about the local polymer dynamics and the segmental motion at the microscopic level.

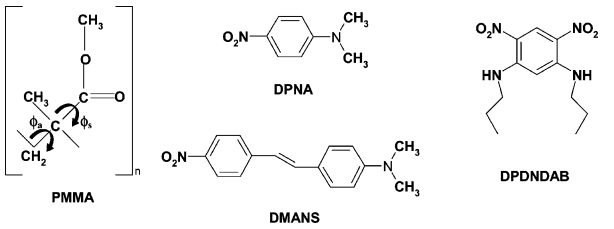

Figure 1. Schematic representation of the PMMA monomer and the definition of its torsional angles ϕ_a and ϕ_s. The structure of the investigated chromophores, dimethyl-*p*-nitroaniline (DPNA), 4-(dimethylamino)-4′-nitrostilbene (DMANS), and *N*,*N*′-dipropyl-2,4-dinitro-1,5-diaminobenzene (DPDNDAB), is also given.

The molecular model and the method of simulations are presented in the next section. Results on thermodynamics, structure, and segmental dynamics are presented and discussed under Results and Discussion, followed by the conclusions drawn from this work.

Molecular Dynamic Simulations

Five equivalent initial structures, for each host−guest system, generated using the Cerius[2] software package,[35] were used in the present work. A unit cell of the investigated system consisted of one isotactic PMMA 90-mer with molecular weight 9012.58 amu and two chromophore molecules. The structures of PMMA and the considered chromophores (dopants) are presented in Figure 1. Every simulated unit cell was cubic with an edge length of 25.11 Å. The corresponding density was 0.98 g/cm^3 for PMMA/DPNA (3.6 wt %) and 1.00 g/cm^3 for PMMA/DMANS (5.6 wt %) and PMMA/DPDNDAB (5.9 wt %). The numbers in parentheses correspond to the mass fractions of the respective chromophores. The obtained densities correspond to the liquid state of the systems. The initial configurations were generated using Amorphous Cell, a module of the Cerius[2] softare package. Each configuration was minimized first by the steepest descent method employing a convergence criterion of 1000 kcal mol^{-1} Å^{-1}, followed by the conjugate gradient method employing a convergence criterion of 10 kcal mol^{-1} Å^{-1}. Thereafter, a NVT molecular dynamics simulation was carried out for 110 ps at 500 K using a step size of 1 fs. The lowest energy configurations of these runs were again minimized by steepest descent and conjugate gradient methods, with a convergence criterion of 0.1 kcal mol^{-1} Å^{-1}.

The simulations were performed using the GROMACS software.[36] The potential energy is computed as a summation of the contributions due to bond stretching, bond bending, dihedral angle torsion, and nonbonded interactions:

$$U = \sum_{\text{all bonds}} U_{\text{bond}}(l_i) + \sum_{\text{all angles}} U_{\text{angle}}(\theta_i) + \sum_{\text{all dihedral angles}} U_{\text{torsional}}(\phi_i) + \sum_{\text{all pairs } i,j} U_{\text{nonbonded}}(r_{ij}) \quad (1)$$

where l_i, θ_i, and ϕ_i refer to bond length, bond angle, and dihedral angle, respectively, and r_{ij} is the distance between atoms i and j. The nonbonded interactions are modeled with the Lennard-Jones 12−6 potential, a Coulombic potential due to fixed partial charges, and an external electric field, if present. The potential energy due to an external field is computed from the expression $\sum_i \vec{r}_i \cdot E q_i$, where i labels the atoms. Bonded interactions are based on a fixed list of atoms. Bond stretching and bond bending are

represented by harmonic potentials, while dihedral angle distortions are modeled by a simple cosine function. As in the work of Kim and Hayden, the all-atom consistent valence force field (CVFF)[37−39] was selected for the present molecular dynamics (MD) study. This force field has been used successfully to model a wide variety of chemical and biophysical systems,[40] including crystalline systems.[41] The force field parameters for the considered molecules are given in the Appendix. The partial charges employed on the chromophores correspond to dipole moments of 3.1 D for DPNA, 10 D for DMANS, and 9 D for DPDNDAB.

The following parameters were employed in this work for all MD simulations: simulation time step was 1 fs, the short-range neighbor list was created employing the grid search method with cutoff distance 0.95 nm, and Lennard-Jones and Coulomb interactions were calculated within the neighbor list employing periodic boundary conditions. The long-range interactions were calculated using the three-dimensional particle-mesh Ewald method (PME).[42,43] The investigated properties give the same results with or without long-range energy and pressure corrections. Consequently, long-range corrections are not taken into account. The energies, coordinates, and velocities were recorded every picosecond. Most simulations were performed in the NVT canonical ensemble using the Nose−Hoover extended ensemble[44,45] to control temperature. A few simulations in the NPT ensemble employing the Rahman−Parrinello[46] method to control the pressure were performed in order to calculate the density.

The geometry-optimized structures were relaxed for 1.5 ns under NVT conditions at 500 K to obtain equilibrated structures. The total energy reached an approximately constant value for all structures after about 1 ns. In addition the unpoled structures have been simulated with a further 1.5 ns run at $T = 500$ K. Then a poling external electric field was applied in the *z*-direction to all systems and a 1.5 ns MD simulation was performed to study the poling process above T_g. For the PMMA/DPNA system, the applied electric field strength was 5 kV/μm, which was found by Kim and Hayden to be adequate to reach a steady state with respect to chromophore orientation in the field.[11] For the PMMA/DMANS system we used the electric field strengths of 5, 10, and 15 kV/μm, and for the PMMA/DPDNDAB system strengths of 5 and 10 kV/μm have been employed. Steady states were obtained only with the largest field values. It should be noted that these field strengths are much higher than those employed in experimental poling alignment, but they are necessary in order to obtain steady states within the time scale of the simulations.[11]

To locate the appropriate temperature for the high-density-state simulations, we estimated the phase transition temperature T_g of the systems. This was done by performing field-free simulations in the isobaric−isothermal (NPT) ensemble at atmospheric pressure and different temperatures starting from 100 K up to 700 K in 100 K increments. At each temperature the systems were first equilibrated for 1.5 ns, succeeded by a further 1.5 ns of production run during which the density was recorded. Subsequently, T_g was estimated from a density−temperature plot as in ref 47. No attempts were made to incorporate possible effects of electron−phonon interactions on T_g.

After establishing that the glass transition temperature is above 300 K, the final configurations of the low-density MD runs, poled with the highest employed field strengths employed, were used in a simulated cooling process from 500 to 300 K in the presence of the poling field, employing the simulated annealing (SA) approach. SA is generally used as an optimization technique particularly well suited to overcome the multiple minima problem.[48,49] During SA, a molecule may cross barriers between conformational energy minima to reach the lowest minimum. SA was used, e.g., to refine protein structures from NMR and X-ray data[50−52] and to locate the global minimum conformation of polypeptides and proteins.[53−55] The two most commonly used cooling protocols are linear slow cooling[56,57] and constant temperature followed by quenching.[58] We have used SA with the MD algorithm in the isobaric−isothermal ensemble[59] with the protocol implemented in GROMACS where the reference temperature is varied linearly. SA with decreasing temperature was performed from 500 to 300 K in the presence of the poling field. A similar approach to simulate crystallization from a liquid inorganic material was used in several works.[60,61] In our case the cooling rate was 1.3×10^{11} K/s. Even at this high rate the atoms in the liquid still have time to readjust to new positions, although a full equilibration may not be achieved. The final densities after SA were 1.182 ± 0.005, 1.173 ± 0.005, and 1.191 ± 0.004 g/cm^3 for PMMA/DPNA, PMMA/DMANS, and PMMA/DPDNDAB, respectively, which is in good agreement with the experimental densities.[62]

The poled, sub-T_g systems were simulated at constant NVT conditions, with poling field applied, for a further 1.5 ns, which were used to analyze the poled, high-density systems. Finally, to investigate the system stability and back-relaxation of the chromophores, the poling field was switched off, and 1.5 ns MD simulations under NVT conditions were performed.

Results and Discussion

Phase Transition Temperature T_g. As explained in the previous section, T_g was determined from the density−temperature dependence, depicted in Figure 2. The T_g values, as estimated from the crossing point of two least-squares line fits at high and low temperatures, are 400 ± 50, 450 ± 50, and 460 ± 60 K for PMMA/DPNA, PMMA/DMANS, and PMMA/DPDNDAB, respectively. For comparison, we performed an additional simulation of pure PMMA and found a T_g of 520 ± 40 K. These data show that our simulations capture the effect of lower glass transition temperature in polymers doped with low molecular weigth dopants as compared to the pure polymer, although the simulated T_g of pure isotactic PMMA is significantly larger than the experimental value of isotactic PMMA (about 330 K [47]). A similar overestimation of T_g of PMMA has been reported by Soldera using the *pcff* force field.[47]

The phase transition at T_g can be also inferred from the temperature dependence of the chromophore translation diffusion coefficient, shown in Figure 3. For all investigated systems the translation diffusion coefficient drastically increases at temperatures above 500 K. No further refinement of T_g was attempted, as the main purpose of the T_g determinations was the establishment of a reference temperature to ensure that all simulations above this temperature would correspond to liquid state simulations, while those below would correspond to glassy state simulations.

Conformational Properties of PMMA. The conformational properties of PMMA were investigated for all simulated systems. Kim and Hayden[11] reported that the population of torsional angles ϕ_a and ϕ_s, defined in Figure 1, is fairly independent of poling conditions in PMMA/DPNA, showing symmetric distributions for both dihedral angles with three highly populated states: near trans, gauche+, and gauche−. We have found that these distributions for the PMMA/DMANS and PMMA/DPDNDAB systems are similar to those for the PMMA/DPNA structure as presented in ref 11. The similarity of the torsion

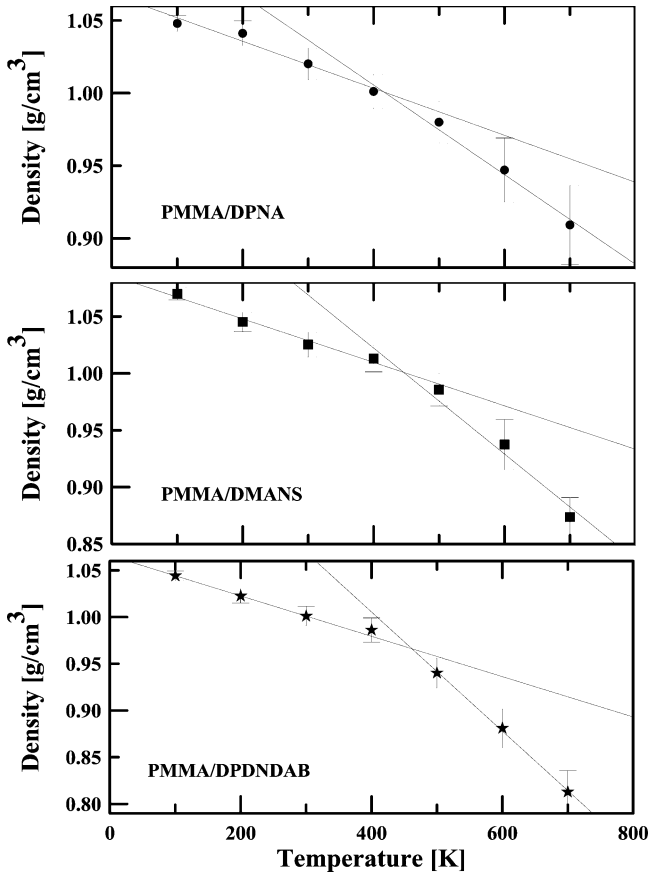

Figure 2. Glass transition temperature predicted by MD simulations for the systems PMMA/DPNA, PMMA/DMANS, and PMMA/DPDNDAB.

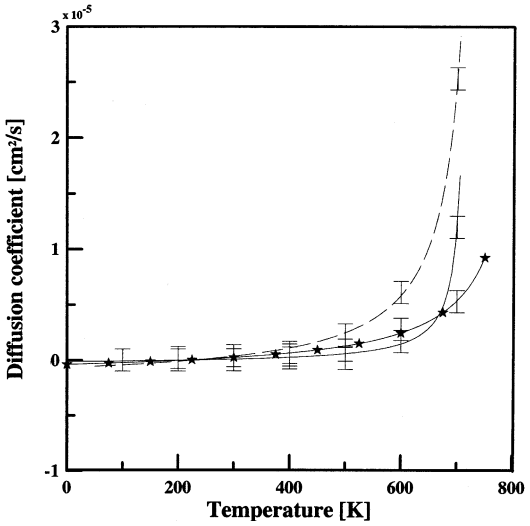

Figure 3. Variation of diffusion coefficient with temperature for the systems PMMA/DMANS (solid line), PMMA/DPNA (dashed line), and PMMA/DPDNDAB (solid line with stars).

angle distribution for all considered host−guest systems permits the conclusion that it is an intrinsic property of PMMA and is not affected by the dopants or the poling process.

The mobility of the polymer can be characterized based on the torsional autocorrelation function (TACF), which is defined by[63]

$$\mathrm{TACF}(t) = \langle \cos(\phi(\tau) - \phi(\tau + t)) \rangle_\tau \qquad (2)$$

where the notation on the right-hand side signifies averaging

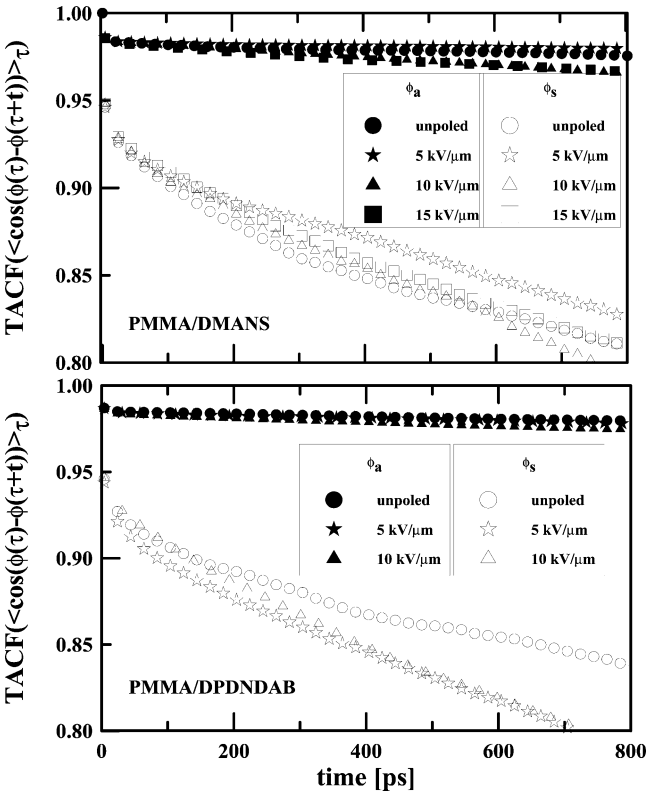

Figure 4. Torsional autocorrelation function of ϕ_a and ϕ_s for PMMA at $T = 500$ K for PMMA/DMANS and PMMA/DPDNDAB systems.

over the time origin τ. The TACFs of ϕ_a and ϕ_s, which are a measure of the backbone and side-chain mobility, were calculated for all systems. In Figure 4, ϕ_a and ϕ_s are shown for DMANS and DNDNDAB at $T = 500$ K for various electric field strengths. As expected, the rotational mobility of the side groups of PMMA is higher than that of the backbone for all simulated structures. The free volume around the side group enables its reorientation. DPDNDAB as a dopant of the unpoled structure appears to decrease the mobility of the polymer chain. Both TACFs of PMMA in the system PMMA/DPDNDAB in the unpoled liquid state decay slower than those of the other host−guest systems. This correlates with the computed T_g value. The decreased mobility of the polymer in PMMA/DPDNDAB, in the unpoled low-density system, may be responsible for the estimated high T_g value, which is the largest among the three systems investigated. Similarly, in the unpoled PMMA/DPNA system the decrease of the TACFs is found to be considerably faster than for the other systems, which correlates well with its lower T_g value. In general, the chromophores decrease T_g of the polymer matrix. One problem with employing host−guest organic materials in electronic devices is that the glass transition temperature of the polymer host may decrease dramatically due to plasticization by the chromophore guest.[64] Our data suggest that PMMA doped with DPDNDAB exhibits the highest thermal stability.

The field affects the local dynamics of PMMA segments and influences the flexibility of the torsional angle motion. Upon closer examination of the TACF of the angle ϕ_a in PMMA/DMANS, we note that, compared with the unpoled state, its flexibility decreases when the electric field of strength 5 kV/μm is applied (Figure 4). Fields of higher strength lead to marginally faster decay of the TACF. The same behavior for this field, albeit more pronounced, is observed for ϕ_s, while the stronger fields nearly reproduce the field-free stiffness. We found, in agreement with Kim and Hayden, that the TACFs of

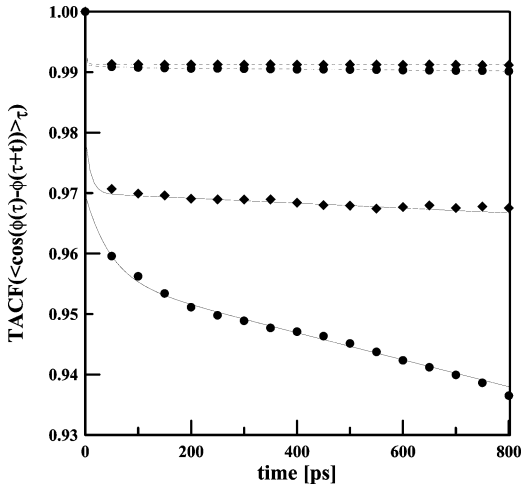

Figure 5. Torsional autocorrelation function of ϕ_a (dashed line) and ϕ_s (solid line) dihedrals of PMMA for the unpoled (●) and poled (◆) structures in the glassy PMMA/DMANS structure ($T = 300$ K). The lines are the results of biexponential fits.

ϕ_a and ϕ_s for PMMA/DPNA decay more slowly as the field increases.[11] The electric field increases the flexibility of both torsional angles of the polymer in PMMA/DPDNDAB (Figure 4). The electric field locks the rodlike molecules, namely DPNA and DMANS, in place, which decreases the flexibility of the polymer. In the case of DPDNDAB the molecule is more internally flexible, and this would allow for greater cooperation with the configurational motion of the polymer. The correlation of the motion of the bonds depends on the intensity of the electric field and on the guest material. The torsional fluctuations of the side groups are correlated with the chromophore reorientation and are probably influenced by the electrostatic guest−host interaction.

The reorientation of side groups is slower in the high-density structure ($T = 300$ K) in comparison to that observed in the low-density one ($T = 500$ K) for all considered structures. This is consistent with observations in pure polymer systems (e.g., Antoniadis et al.[65]). Additionally, in the high-density systems the decay of the TACF of ϕ_s increases following the removal of the poling field as shown for PMMA/DMANS in Figure 5. Similar behavior is found for all the polymer/dopant systems. This shows that the external field leads to higher correlated mobility of the side groups. The side group mobility is more closely related to the chromophore reorientation than is the configurational motion of the backbone units. The TACF of ϕ_s cannot be fitted by a purely exponential function at both simulated temperatures for all systems. Similar behavior has been reported for *n*-$C_{44}H_{90}$ melts by Smith et al.[66]

Static Properties of Dopants. The spatial distribution of the chromophores was investigated based on intermolecular radial distribution functions (RDFs). For DPNA and DMANS the center of mass (COM) of the nitro group and the dimethylamino group was considered, while for DPDNDAB the COMs of the nitro group and the methyl group at the end of the alkyl chain were taken into account. For PMMA the COMs of four groups were used: COO, CH_2, bCH_3 (methyl group bonded to the backbone α-carbon atom), and sCH_3 (methyl group bonded to COO). The COMs of the different groups were calculated for each snapshot. The RDF was calculated according to the expression

$$g_{AB}(r) = \frac{\langle \rho_B(r) \rangle}{\langle \rho_B \rangle_{loc}} = \frac{1}{\langle \rho_B \rangle_{loc}} \frac{1}{N_A} \sum_{i \in A}^{N_A} \sum_{j \in B}^{N_B} \frac{\delta(r_{ij} - r)}{4\pi r^2} \qquad (3)$$

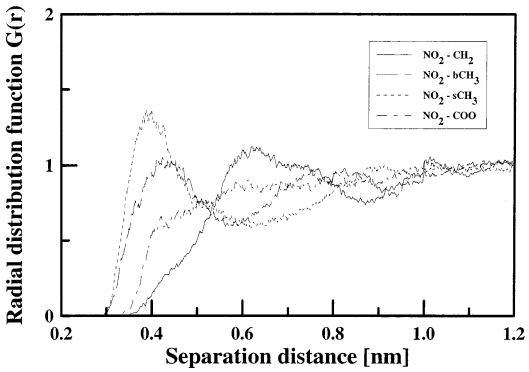

Figure 6. Partial radial distribution function between the center of mass of NO_2 of DPDNDAB and different subunits of PMMA at $T = 500$ K.

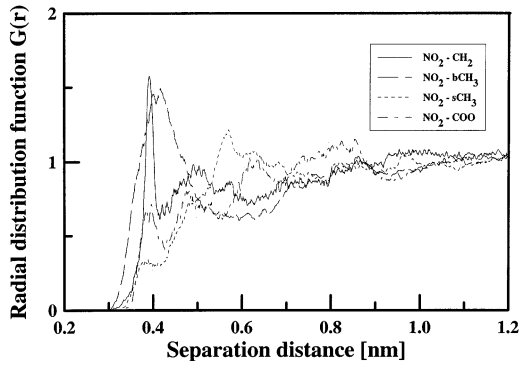

Figure 7. Partial radial distribution function between the center of mass of NO_2 of DMANS and different subunits of PMMA at $T = 500$ K.

where $\langle \rho_B(r) \rangle$ is the density of group B at distance r around group A, and $\langle \rho_B \rangle_{loc}$ is the density of group B averaged over the sphere around group A with the highest value of distance between particles r_{max}, which is equal to half the unit cell length. Representative RDFs for the considered structures at $T = 500$ K and $T = 300$ K are presented in Figures 6−8. Each RDF is an average over five independent runs for each system.

Figure 6 presents the RDF between the nitro group of DPDNDAB and groups of PMMA for the low-density structure. Kim and Hayden have reported similar results for PMMA/DPNA.[11] DPNA and DPDNDAB are located closer to the side groups than to the backbone units in the liquid state system. The first maximum in the RDF of the nitro group of DPDNDAB and the side methyl group occurs at 0.4 nm, similar to the PMMA/DPNA[11] mixture, while the first peak in the RDF of NO_2 and the CH_2 group occurs at ca. 0.6 nm. Analogous results were obtained for the dimethylamino group of DPDNDAB.

DMANS is located closer to the backbone. Figure 7 shows a very narrow first peak at 0.4 nm for the RDF of NO_2-CH_2 and a broader one in the RDF of NO_2-bCH_3. In the RDF of NO_2-sCH_3 a very small peak occurs at 0.4 nm and a much larger at about 0.6 nm. Similar observations have been made for the dimethylamino group of DMANS. No long-range order exists for separation distances higher than 0.6 nm. The observed RDFs are typical for amorphous structures. We have found that the RDFs of poled structures in the melt are similar to those of the unpoled ones. The external electric field does not impose any long-range order inside the polymer/dopant structure.

The RDFs in the glassy state show a different behavior. The broad peak at 0.5 nm in the RDF of $N(CH_3)_2-sCH_3$ of DPNA in the low-density system is split into two peaks: one at about 0.4 nm and the second at about 0.5 nm (Figure 8). The RDFs

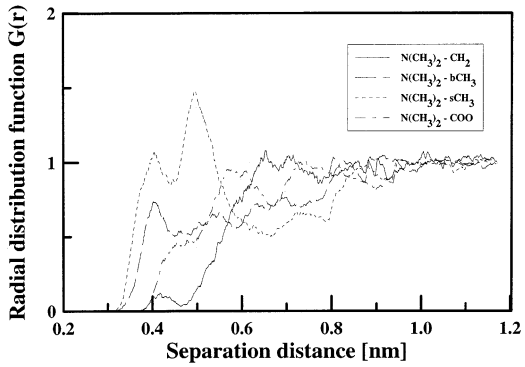

Figure 8. Partial radial distribution function between the center of mass of $N(CH_3)_2$ of DPNA and different subunits of PMMA at $T = 300$ K.

of PMMA/DPDNDAB at $T = 300$ K are similar to those of PMMA/DMANS at the same temperature. However, in the liquid state the arrangement of the chromophores in PMMA/DPDNDAB is in closer agreement with that of PMMA/DPNA. In the high-density state DMANS and DPDNDAB are located closer to the backbone units of the polymer (for which the mobility is lower) than to the side groups. The location of the DMANS and DPDBDAB in the system at $T = 300$ K additionally influences the stability of the alignment. Thus, the reorientation of DMANS and DPDNDAB, following removal of the electric field, should be slower than that of DPNA.

Dopant Reorientation. The field-induced reorientation of the dopant molecules was investigated by computing $\cos \theta(t)$, where $\theta(t)$ is the time-dependent angle between the dipole moment of the chromophore and the external electric field. The degree of alignment depends on the electric field strength and the spatial extension of the dipolar molecules. The values of $\cos \theta(t)$ are presented in Figures 9−11. These values have been computed by averaging over five structures, each of which involves two chromophores. We note that the poling field was switched on at the start of the liquid state simulations; the corresponding curves in Figures 9−11 start therefore from the equilibrated values of the unpoled structures, i.e., at around zero. The glassy state simulations on the other hand start from structures obtained from the simulated annealing process with applied poling field and start therefore from much larger values of $\cos \theta$. The partial charges used in the simulations have been employed to calculate the dipole moments; no induced effects have been considered. In the unpoled low-density system the dipole moments are approximately random. The fluctuations in DPNA (Figure 9) are much larger than those in DMANS (Figure 10) and in DPDNDAB (Figure 11). This is due to the much smaller size of the DPNA molecule as compared to DMANS and DPDNDAB, which leads to a higher mobility. The reorientational movements of DMANS and DPDNDAB are essentially restricted to rotations around the dipole moment axis.

The orientation of the dipoles by the field in the steady state is governed by the Boltzmann distribution $f \sim \exp(-\vec{\mu}\cdot\vec{E}/kT)$, where $\vec{\mu}\cdot\vec{E}$ is the scalar product of molecular dipole moment $\vec{\mu}$ with the external electric field $\vec{E}$, k is Boltzmann's constant, and T is the temperature. The order parameters $\langle \cos \theta \rangle$ and $\langle \cos^3 \theta \rangle$ computed over the Boltzmann distribution are[30]

$$\langle \cos \theta \rangle = \coth p - \frac{1}{p} = L_1(p) \tag{4}$$

$$\langle \cos^3 \theta \rangle = \left(1 + \frac{6}{p^2}\right) L_1(p) - \frac{2}{p} = L_3(p) \tag{5}$$

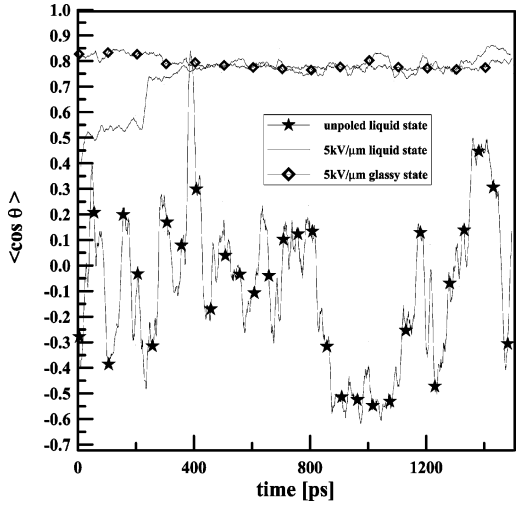

Figure 9. Variation of $\langle \cos \theta \rangle$, where θ is the angle between the dipole moment of DPNA and the field direction, with the poling time. Electric field poled and unpoled structures are considered.

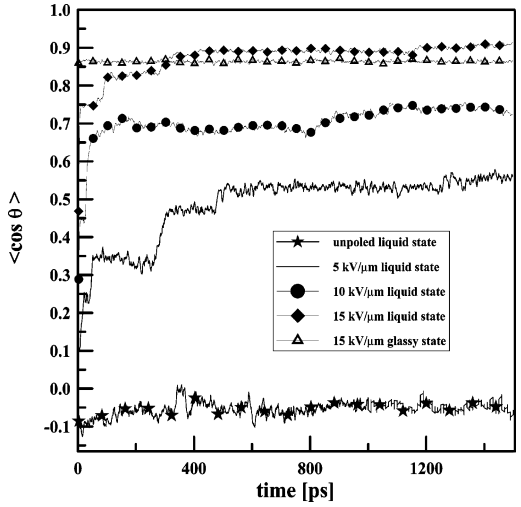

Figure 10. Average value of the dipole moment vector of DMANS, along the field direction, for electric field poled and unpoled structures.

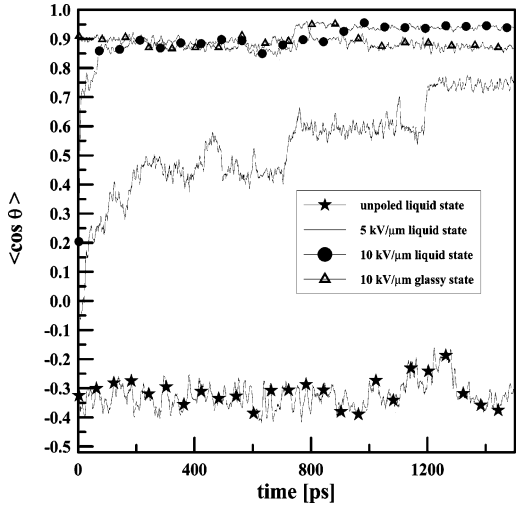

Figure 11. Average value of the dipole moment vector of DPDNDAB, along the field direction (z-axis), for electric field poled and unpoled structures.

where $p = \vec{\mu}\cdot\vec{E}/kT$ and $L_1(p)$ and $L_3(p)$ are odd-order Langevin functions. In Table 1 we compare the order parameters obtained for the Boltzmann distribution with those computed from the

TABLE 1: Order Parameters $\langle\cos\theta\rangle$ and $\langle\cos^3\theta\rangle$ Calculated from MD Simulations and the Theoretically Predicted Values $L_1(p)$ and $L_3(p)$

	DPNA		DMANS				DPDNDAB		
	liquid state, $T = 500$ K	glassy state, $T = 300$ K	liquid state, $T = 500$ K			glassy state, $T = 300$ K	liquid state, $T = 500$ K		glassy state, $T = 300$ K
order params	5 kV/μm	5 kV/μm	5 kV/μm	10 kV/μm	15 kV/μm	15 kV/μm	5 kV/μm	10 kV/μm	10 kV/μm
$L_1(p)$	0.86	0.92	0.96	0.98	0.99	0.99	0.95	0.97	0.98
$L_3(p)$	0.68	0.79	0.86	0.94	0.95	0.97	0.87	0.93	0.96
$\langle\cos\theta\rangle$	0.85 ± 0.10	0.79 ± 0.16	0.56 ± 0.28	0.73 ± 0.15	0.91 ± 0.08	0.86 ± 0.14	0.74 ± 0.18	0.94 ± 0.06	0.91 ± 0.08
$\langle\cos^3\theta\rangle$	0.61 ± 0.18	0.50 ± 0.23	0.17 ± 0.38	0.40 ± 0.25	0.76 ± 0.20	0.66 ± 0.27	0.41 ± 0.23	0.83 ± 0.14	0.74 ± 0.19

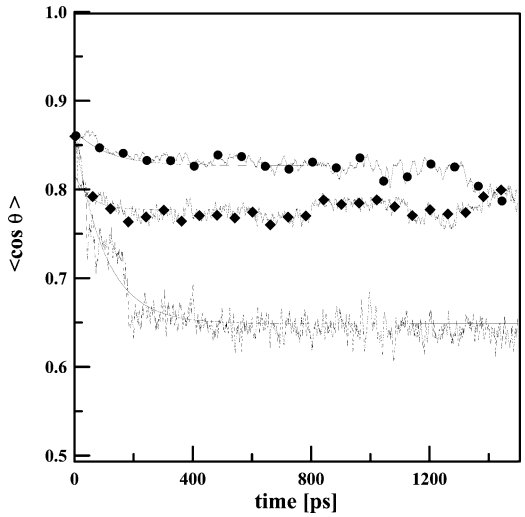

Figure 12. Calculated average value of $\langle\cos\theta\rangle$, where θ is the angle between the dipole moment vector of chromophore and the field direction, for DPNA (solid line), DMANS (line with diamonds), and DPDNDAB (line with circles), for glassy system. The lines are the results of biexponential fits.

MD simulations, where for the poled systems, at $T = 500$ K, the last 100 ps was taken into account. For the systems at $T = 300$ K with the highest fields applied (5, 15, and 10 kV/μm for DPNA, DMANS, and DPDNDAB, respectively) 1500 ps was used. The order parameters for the simulated systems at $T = 500$ K, with the highest electric fields applied, are in good agreement with those calculated from a Boltzmann distribution, showing that the simulated systems are in thermal equilibrium with respect to the external field. The increase of the field strength, which is necessary to achieve a steady state distribution for the chromophores, follows the order DPNA < DPDNDAB < DMANS, and it is due to the increasing extension and stiffness of the molecules in this order, leading to increasing resistance to reorientation of the dipolar axis. The employed time (1.5 ns) of the MD simulations is not sufficient to obtain steady state distribution of the considered chromophores, applying the electric field 5 kV/μm for PMMA/DPDNDA system and 5 or 10 kV/μm for PMMA/DMANS. The order of alignment achieved in the low-density poling process is approximately preserved during the simulated cooling (Table 1). In consequence, the glassy state simulations start from a state where the chromophores are already partially aligned by the poling field. This is in contrast to the approach used by Kim and Hayden,[11] who tried to simulate the glassy state in the poling field by starting from a completely unpoled structure, and had to employ very high poling fields (up to 50 kV/μm) to overcome the strongly reduced chromophore reorientational mobility in the glassy state. As a consequence, the order parameters obtained for PMMA/DPNA using an electric field of 5 kV/μm at $T = 300$ K in our approach are in much better agreement with those calculated from a Boltzmann distribution than those of Kim and Hayden, using the same field strength, who obtained for example for $\langle\cos\theta\rangle$ a value of 0.18 ± 0.01. However, the high-density data in Table 1 show that the average values obtained from our simulation are still a bit lower than those to be expected from a Boltzmann distribution. The reason for this is probably that

TABLE 2: Relaxation Times Computed for the Three Considered Systems from the $\langle\cos\theta\rangle$ Decay Curve

system	temp (K)	τ_1 (ps)	τ_2 (ps)
DPNA/PMMA	300	2.2×10^7	107.1
DMANS/PMMA	300	704.2×10^7	62.2
DPDNDAB/PMMA	300	720.8×10^7	110.6
DPNA/PMMA	500	726.3	102.4
DMANS/PMMA	500	7781.2	61.7
DPDNDAB/PMMA	500	1212.3	111.7

TABLE 3: $U_{bond} = (1/2)K_l(r - r_0)^2$

bond	r_0 (nm)	K_l (kJ mol^{-1} nm^{-2})
C(Ar)−C(Ar)	0.1340	401 817.6
C(Ar)−H	0.1080	304 222.8
C(Ar)−N′	0.1472	294 040.9
C(Ar)−N	0.1420	234 393.6
N′−O	0.1218	469 619.3
N−C	0.1460	316 075.6
C−H	0.1105	285 138.0
C(Ar)−C′	0.1472	294 040.7
C′−C′	0.1330	548 481.0
C′−H	0.1080	304 222.8
C−O	0.1425	228 701.0
O−C(COO)	0.1370	334 848.0
C(COO)−O′	0.1230	515 098.0
C(COO)−C	0.1520	236 982.0
C−C	0.1526	270 152.0
N−H	0.1026	404 706.7

TABLE 4: $U_{angle} = (1/2)K_\vartheta(\vartheta - \vartheta_0)$

angle	ϑ_0 (deg)	K_ϑ (kJ mol^{-1} rad^{-2})
O−N′−O	120.0	950.742
O−N′−C(Ar)	120.0	456.230
N′−C(Ar)−C(Ar)	120.0	290.313
C(Ar)−C(Ar)−C(Ar)	120.0	753.408
H−C(Ar)−C(Ar)	120.0	309.734
N−C(Ar)−C(Ar)	120.0	853.862
C−N−C	120.0	309.734
C−N−C(Ar)	120.0	418.560
N−C−H	109.5	431.117
H−C−H	106.4	330.662
C′−C(Ar)−C(Ar)	120.0	290.312
H−C′−C′	121.2	282.947
H−C′−C(Ar)	110.0	371.681
C(Ar)−C′−C′	122.3	303.037
H−C−O	109.5	477.158
C(COO)−O−C	109.5	502.272
O′−C(COO)−O	123.0	1213.824
H−C−C	110.0	371.681
C−C(COO)−O	110.0	1027.983
C−C(COO)−O′	120.0	569.242
N−C−C	109.5	418.560
N−C−H	109.5	431.117
C−C−C	110.5	390.098
H−N−C	122.0	292.992
H−N−C(Ar)	115.0	313.920

TABLE 5: $U_{\text{dihedral}} = K_\phi(1 + \cos(n\phi - \phi_0))$

dihedral	ϕ_0 (deg)	n	K_ϕ (kJ mol^{-1})
C(Ar)−N−C−X	0.0	0	0.000
X−C(Ar)−N−X	180.0	2	41.856
C(Ar)−C(Ar)−N′−O	180.0	2	41.856
X−C(Ar)−C(Ar)−X	180.0	2	50.227
C′∠C′∠C(Ar)−C(Ar)	180.0	2	41.856
X−C′−C′−X	180.0	2	68.225
C−C−C(COO)−O′	180.0	2	41.856
X−C−C−X	0.0	3	5.956
C−C−C(COO)−O	0.0	0	0.000
O′−C(COO)−O−C	180.0	2	18.835
C(COO)−O−C−H	0.0	3	1.632

TABLE 6: $U_{\text{oop}} = K_\lambda(1 + \cos(n\lambda - \lambda_0))$

	λ_0 (deg)	n	K_λ (kJ mol^{-1})
O−N′−O−C(Ar)	180.0	2	41.856
C(Ar)−C(Ar)−C(Ar)−X	180.0	2	1.549
C(Ar)−N−C−C	180.0	2	0.209
C−C(COO)−O′−O	180.0	2	48.553

TABLE 7: Lennard-Jones (12−6) Parameters[a]

	A_i [kJ/(mol Å^{12})]	B_i [kJ/(mol Å^6)]
C	7 493 650.1	2212.0142
C(Ar), C′	12 426 014.1	5548.8838
O	1 142 228.4	2088.1071
N	9 488 221.1	5150.6194
H	29 753.2	137.5840

[a] Cross terms are computed according to $A_{ij} = (A_iA_j)^{1/2}$ and $B_{ij} = (B_iB_j)^{1/2}$.

the time scale used for the simulated cooling does not allow for the additional relaxation necessary to reach the steady state in the high-density systems.

The back-relaxation of chromophores at $T = 300$ K to the unpoled state after switching off the external field, as measured by $\cos\theta(t)$, was found to be solute dependent, as shown in Figure 12. As expected, the relaxation of DPNA is fastest among the three systems. More surprising is that DMANS relaxes faster than DPDNDAB, although the differences are not large.

The decay of the value of $\cos\theta$ corresponds to the reorientation of the dopants and is correlated to the time decay of the SHG output signal. We observe a "fast" decay at short times and a "slow" decay at long times. Consequently, the data cannot be fit according to a single-exponential Debye relaxation model. Attempts to use a biexponential function $\cos\theta(t) = A\exp(-t/\tau_1) + B\exp(-t/\tau_2)$ are more successful and lead to a term which is nearly constant over the time period used for the fit, and a second term with a relaxation time of ∼100 ps (see Table 2), which may be due to rotational relaxation in residual free volume. To establish that this is not just an artifact arising from the nonequilibrated nature of the high-density systems, we performed additional field-free simulations starting from the equilibrated poled low-density systems. Analyzing the decay of $\cos\theta(t)$ in the same way as that of the high-density systems, we found very similar short-time relaxation times for the three systems (Table 2). This shows that the short-time relaxation in the high-density systems is not an artifact and additionally that it is also independent of the density. The decay of the SHG signal has been investigated experimentally on much longer time scales than used here, and it has been found generally that satisfactory fits are obtained only with multiexponential functions.[13,19,28]

Conclusions

In this work we studied the dipole moment reorientation of DPNA, DMANS, and DPDNDAB incorporated in PMMA matrix during the poling process. To the best of our knowledge, it is one of the first simulation studies investigating relaxation of the chromophores following the removal of the external poling electric field. We have used fully atomistic modeling to study the alignment of the chromophores and a solidification of the guest−host nonlinear polymer. We have applied a different approach to obtain the glassy poled structures by simulating the cooling process by simulated annealing. New high-density structures at $T = 300$ K were obtained by performing phase transition simulations. During the simulated cooling process the degree of alignment of dopants was preserved. This allowed the application of the same field strengths in the glassy state as in the liquid state, in contrast to previous approaches where both states were poled independently and the field strengths in the glassy state had to be much larger than in the liquid state.

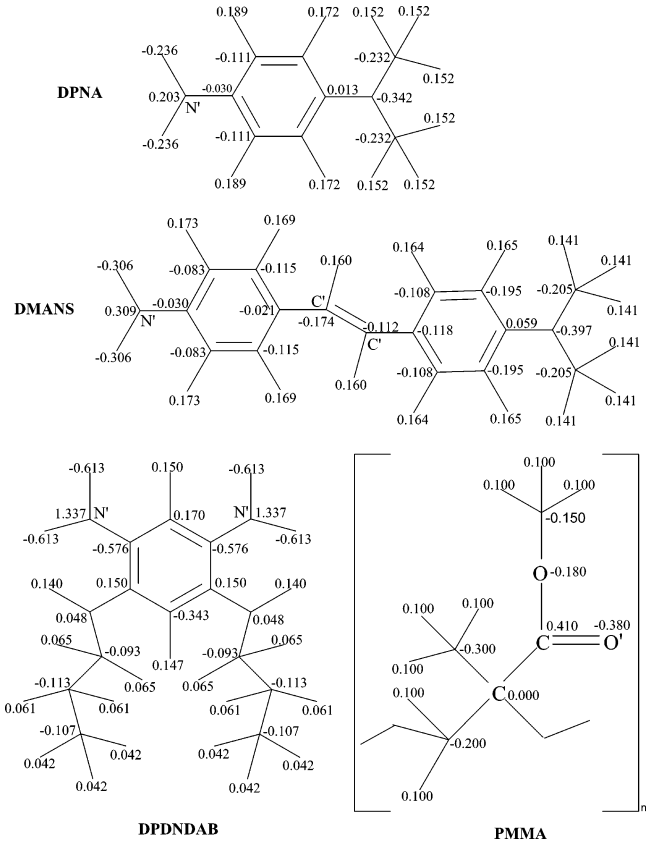

Figure 13. Charges of PMMA and the considered chromophores employed for the MD simulations. One unit of charge is equal to 1.6 × 10^{-19} C.

For all the considered systems at $T = 500$ K poled with the highest electric field, the order parameters $\langle\cos\theta\rangle$ and $\langle\cos^3\theta\rangle$ are in agreement with the odd-order Langevin functions $L_1(p)$ and $L_3(p)$. Saturation of the field-induced dipole moment alignment has been achieved for the applied electric fields, and the considered structures are approximately in a steady state even for $T = 300$ K.

No significant differences in the static conformational properties of the polymer were observed between poled and unpoled structures in the liquid and glassy states for all structures. The conformational behavior of the PMMA molecular groups depends on the solute. DPNA prefers to be located closer to the polymer side groups than to the backbone units for both the liquid and glassy states, and the reorientation of this chromophore is fast even in the absence of an electric field. DMANS molecules are located closer to backbone units of

PMMA, the mobility of which is lower than that of the side groups. The time of back-relaxation of aligned DMANS is long. DPDNDAB chromophores are located near the side groups of the polymer in the liquid state, and they can be aligned relatively easily taking their size into consideration, with a moderate electric field. In the glassy state DPDNDAB chromophores prefer to be located near the backbone units of PMMA and their mobility is decreased.

The decay of chromophore alignment following the electric field removal cannot be fitted by a single-exponential function. Biexponential fits lead to a nearly constant term and a second one, which may be due to rotational relaxation in local free volume. The fast short-time relaxation of DMANS may be connected to electrostatic interaction between the chromophore and side groups of polymer. DMANS has the highest dipole moment, and the electrostatic interaction with the polymer is relatively strong in comparison with DPNA and DPDNDAB.

From the considered systems, PMMA/DPDNDAB is the most interesting guest−host material from the thermodynamics and mechanical points of view. It has the best thermal stability, and its chromophore reorientation is relatively long. The NLO properties of the dopants in the studied guest−host poled systems are under investigation.

Acknowledgment. M.G.P. acknowledges a Marie Curie Host Development Fellowship (HPMD-CT-2001-00091). M.M.-J., who was the Marie Curie Fellow, is grateful for her grant.

Appendix

Potential parameters used for the MD simulations are included in Tables 3−7. The atoms are defined in Figure 13. In the tables, C(Ar) denotes aromatic carbon atoms.

References and Notes

(1) *Polymers for Lightwave and Integrated Optics: technology and Applications*; Hornak, L. A., Ed.; Marcel Dekker: New York, 1992.
(2) Garito, A. F.; Shi, R. F.; Wu, M. H. *Phys. Today* **1994**, *47*, 51.
(3) Dulcic, A.; Sauteret, C. *J. Chem. Phys.* **1978**, *69*, 3453.
(4) Lee, J. Y.; Kim, K. S.; Mhin, B. J. *J. Chem. Phys.* **2001**, *115*, 9484.
(5) Cho, Y. S.; Lee, J. S.; Cho, G.; Wada, T.; Sasabe, H. *Polymer* **2001**, *42*, 9379.
(6) Kuo, W. J.; Hsiue, G. H.; Jeng, R. J. *J. Mater. Chem.* **2002**, *12*, 868.
(7) Meredith, G. R.; van Dusen, J.; Williams, D. J. *Macromolecules* **1982**, *15*, 1385.
(8) Singer, K. D.; Sohn. J. E.; Lalama, S. *Appl. Phys. Lett.* **1986**, *49*, 248.
(9) Wei, S.; Zhenyu, Z.; Qiwei, P.; Qingtian, G.; Lina, Y.; Changshui, F.; Dong, X.; Hongzhen, W.; Jinzhong, Y. *Macromolecules* **2001**, *34*, 2002.
(10) *Nonlinear Optical Properties of Organic Molecules and Crystals*; Chemla, D. S., Zyss, J., Eds.; Academic Press: New York, 1987.
(11) Kim, W.-K.; Hayden, L. M. *J. Chem. Phys.* **1999**, *111*, 5212.
(12) Hampsch, H. L.; Yang, J.; Wong, G. K.; Torkelson, J. M. *Polym. Commun.* **1989**, *30*, 40.
(13) Goodson, T.; Wang, H. *Macromolecules* **1993**, *26*, 1837.
(14) Teraoka, I.; Jungbauer, D.; Reck, B.; Yoon, D. Y.; Twieg, R.; Willson, C. G. *Appl. Phys.* **1991**, *69*, 2568.
(15) Walsh, C. A.; Burland, D. M.; Lee, V. Y.; Miller, R. D.; Smith, B. A.; Twieg, R. J.; Volksen, W. *Macromolecules* **1993**, *26*, 3720.
(16) Schussler, S.; Richert, R.; Bassler, H. *Macromolecules* **1994**, *24*, 4318.
(17) Kohler, W.; Robello, D. R.; Dao, P. T.; Willand, C. S.; Williams, D. J. *J. Chem. Phys.* **1990**, *93*, 9157.
(18) Kim, W.-K.; Hayden, L. M. *Macromolecules* **2000**, *33*, 5747.
(19) Dhinojwala, A.; Wong, G. K.; Torkelson, J. M. *Macromolecules* **1993**, *26*, 5943.
(20) Hayden, L. M.; Kim, W.-K.; Chafin, A. P.; Lindsay, G. A. *J. Polym. Sci Part B: Polym. Phys.* **2001**, *39*, 895.
(21) Brower, S. C.; Hayden, L. M. *J. Polym. Sci. Part B: Polym. Phys.* **1998**, *36*, 1013.
(22) Dhinojwala, A.; Wong, G. K.; Torkelson, J. M. *Macromolecules* **1992**, *25*, 7395.
(23) Strutz, S. J.; Brower, S. C.; Hayden, L. M. *J. Polym. Sci. Part B: Polym. Phys.* **1998**, *36*, 901.
(24) Hooker, J. C.; Torkelson, J. M. *Macromolecules* **1995**, *28*, 7683.
(25) Debye, P. *Polar Molecules*; Lancaster Press Inc.: PA, 1929.
(26) Kohlrausch, F. *Pogg. Ann. Phys.* **1863**, *199*, 352.
(27) Williams, G.; Watts, D. C. *Faraday Soc.* **1971**, *66*, 80.
(28) Hampsch, H. L.; Yang, J.; Wong, G. K.; Torkelson, J. M. *Macromolecules* **1990**, *23*, 3640.
(29) Liu, L.-Y.; Ramkrishna, D.; Lackritz, H. S. *Macromolecules* **1994**, *27*, 5987.
(30) Williams, D. J. Nonlinear Optical Properties of Guest−Host Polymer Structures. In *Nonlinear Optical Properties of Organic Molecules and Crystals*; Chemla, D. S., Zyss, J., Eds.; Academic Press: New York, 1987.
(31) Borbulevych, O. Ya.; Clark, R. D.; Romero, A.; Tan, L.; Antipin, M. Yu.; Nesterov, V. N.; Cardelino, B. H.; Moore, C. E.; Sanghadasa, M.; Timofeeva, T. V. *J. Mol. Struct.* **2002**, *604*, 73.
(32) Nalwa, H. S.; Watanabe, T.; Ogino, K.; Sato, H.; Miyata, S. *J. Mater. Sci.* **1998**, *33*, 3699.
(33) Hampsch, H. L.; Yang, J.; Wong, G. K.; Torkelson, J. M. *Macromolecules* **1998**, *21*, 528.
(34) Dhinojwala, A.; Wong, G. K.; Torkelson, J. M. *Macromolecules* **1992**, *25*, 7395.
(35) www.accelrys.com/cerius2/.
(36) Berendsen, H. J. C.; van der Spoel, D.; van Drunen, R. *Comput. Phys. Commun.* **1995**, *91*, 43. Lindahl, E.; Hess, B.; van der Spoel, D. *J. Mol. Modell.* **2001**, *7*, 306. van der Spoel, D.; van Buuren, A. R.; Apol, E.; Tieleman, P. J.; Sijbers, A. L. T. M.; Hess, B.; Feenstra, K. A.; Lindahl, E.; van Drunen R.; Berendsen, H. J. C. *GROMACS−user manual*; Department of Biophysical Chemistry, University of Groningen: Groningen, Germany, 2002.
(37) Hagler, A. T.; Huler, E.; Lifton, S. *J. Am. Chem. Soc.* **1974**, *96*, 5319.
(38) Kitson, D. H.; Hagler, A. T. *Biochemistry* **1988**, *27*, 5246.
(39) Dauber-Osguthorpe, P.; Roberts, V. A.; Osguthorpe, D. J.; Wolff, J.; Genest, M.; Hagler, A. T. *Proteins: Struct., Funct., Genet.* **1988**, *4*, 31.
(40) Lau, K. F.; Alper, H. E.; Thacher, T. S.; Stouch, T. R. *J. Phys. Chem.* **1994**, *98*, 8785.
(41) Ma, B.; Lii, J. H.; Chen, K.; Allinger, N. L. *J. Am. Chem. Soc.* **1997**, *119*, 2570.
(42) Darden, T.; York, D.; Pedersen, L., *J. Chem. Phys.* **1993**, *98*, 10089.
(43) Essmann, U.; Perera, L.; Berkowitz, M. L.; Darden, T.; Lee, H.; Pedersen, L. G. *J. Chem. Phys.* **1995**, *103*, 8577
(44) Nose, S. *Mol. Phys.* **1984**, *52*, 255.
(45) Hoover, G. W. *Phys. Rev. A* **1985**, *31*, 1695.
(46) Parrinello, M.; Rahman, A. *J. Appl. Phys.* **1981**, *52*, 7182.
(47) Soldera, A. *Polymer* **2002**, *43*, 4269.
(48) Kirkpatrick, S.; Gelatt, C. D.; Vecchi, M. P. *Science* **1983**, *220*, 671.
(49) Larrhoven, P. J. M.; Aarts, E. H. L. *Simulated Annealing: Theory and Aplications*; Reidel Publishing Company: Dordrecht, Germany, 1987.
(50) Nilges, M.; Clore, G. M.; Gronenborn, A. M. *FEBS Lett.* **1988**, *229*, 317.
(51) Brunger, A. T.; Karplus, M.; Petsko, G. A. *Acta Crystallogr., Sect. A* **1989**, *45*, 50.
(52) Brunger, A. T. *J. Mol. Biol.* **1988**, *203*, 803.
(53) Wilson, S. R.; Cui, W.; Moskowitz, J. W.; Schmidt, K. E. *Tetrahedron Lett.* **1988**, *29*, 4373.
(54) Kawai, H.; Kikuchi, T.; Okamoto, Y. *Protein Eng.* **1989**, *3*, 85.
(55) Huong, X.; Moy, F.; Powers, R. *Biochemistry* **2000**, *39*, 13365.
(56) Brunger, A. T.; Krukowski, A.; Erikson, J. *Acta Crystallogr., Sect. A* **1990**, *46*, 585.
(57) Brunger, A. T.; Adams, P. D.; Rice, L. M. *Structure* **1997**, *5*, 325.
(58) Bhattacharya, K. K.; Sethna, J. P. *Phys. Rev. E* **1998**, *57*, 2553.
(59) Lindahl, E.; Hess, B.; van der Spoel, D. *J. Mol. Modell.* **2001**, *7*, 306.
(60) Watanabe, M. S.; Tsumuraya, K. *J. Chem. Phys.* **1987**, *87*, 4891.
(61) Hui, L.; Guanghou, W.; Jijun, Z.; Xiufang, B. *J. Chem. Phys.* **2002**, *116*, 10809.
(62) Sane, S. B.; Cagin, T.; Goddard, W. A.; Knauss, W. G. *J. Comput.-Aided Mater.* **2002**, *8*, 87.
(63) van der Spoel, D.; Berendsen, H. J. C. *Biophys. J.* **1997**, *72*, 2032.
(64) Burland, D. M.; Miller, R. D.; Walsh, C. A. *Chem. Rev.* **1994**, *94*, 31.
(65) Antoniadis, S. J.; Samara, C. T.; Theodorou, D. N. *Macromolecules* **1998**, *31*, 7944.
(66) Smith, G. D.; Yoon, D. Y.; Zhu, W.; Ediger, M. D. *Macromolecules* **1994**, *27*, 5563.